Journal of Nonlinear Optical Physics and Materials
Vol. 5. No. 2 (1996) 205–222

BELOW BAND-GAP NONLINEAR OPTICAL PROPERTIES OF SEMICONDUCTOR-DOPED GLASSES

G. P. BANFI, V. DEGIORGIO, D. FORTUSINI, and H. M. TAN*
Dipartmento di Elettronica, Universitá di Pavia, 27100 Pavia, Italy

Received 6 August 1995

Through nonlinear transmission and wave-mixing measurements, combined with structural data from neutron scattering, we obtain the below band-gap third-order susceptibility $\chi^{(3)}$ (both imaginary and real part) and the refractive-index-change per carrier of semiconductor nanocrystals embedded in a glass matrix. Our data covers a range of crystal radii between 2 and 14 nm, and a range of ratios $y = E_g/(\hbar\omega)$, where E_g is the energy gap of the semiconductor and $\hbar\omega$ is the energy of the incident photon, between 1.1 and 1.9. The magnitude of $\chi^{(3)}$ and its dependence on y are comparable to those of related bulk semiconductors.

1. Introduction

In the last few years much attention was devoted to the effect of quantum confinement on near-resonant optical nonlinearities in semiconductors.[1] Semiconductor doped glasses (SDGs)[1] were the most investigated materials, because of the possibility of obtaining crystallites of very small size with a relatively simple fabrication procedure, and also because of their potential in nonlinear optical devices.[2,3] However, in order to build a device with fast responses and limited losses, one should try to work at frequencies below band-gap. In this transparency range, the question is whether and how the bound-charge nonlinear refraction and the two-photon absorption coefficient (accounted for, respectively, by the real and imaginary parts of $\chi^{(3)}$, the third-order susceptibility) are modified by the nanosize of the crystallites. For frequencies still in the transparency range but above mid-gap, the electron-hole (e-h) pairs generated by two-photon absorption (TPA) can also cause a nonlinear refraction which manifests itself through a fifth order nonlinearity.[4] All these processes are now fairly well understood in bulk semiconductors,[5–7] whereas for SDGs the characterization of the nonlinear optical response below-band-gap is in a more primitive stage.

*Permanent address: Changchun Institute of Optics and Fine Mechanics, Academia Sinica, China.
PACS Nos.: 42.70.Nq;42.65.R; 78.65 Fa

Some calculations suggesting a rather large effect of quantum confinement on both the real and imaginary parts of $\chi^{(3)}$ were presented by Cotter *et al.*[8] The few available experimental data[8–12] published before our works did not permit to draw a clear picture of the situation. The TPA measurements reported in Refs. 8–10 would indicate that the magnitude of $\mathrm{Im}\,\chi^{(3)}$ for the crystallites is typically 2–10 times larger than for the bulk semiconductor. Some experiments were more concerned with the dispersion of $\mathrm{Im}\,\chi^{(3)}$ than its absolute value.[10,11] Kang *et al.*[11] presented TPA spectra derived from luminescence data, and pointed out the necessity to include valence band mixing in the calculation of the energy levels of nanocrystals. Concerning $\mathrm{Re}\,\chi^{(3)}$, Ref. 8 reported measured values about 10–20 times larger than for an undoped borosilicate glass. An even larger figure for $\mathrm{Re}\,\chi^{(3)}$ was derived in Ref. 12. By taking into account that the typical volume fraction of the crystallites in SDGs was in the range 0.1–0.5%,[13] these figures would suggest that $\mathrm{Re}\,\chi^{(3)}$ was significantly larger in nanocrystals than in bulk semiconductors.

In order to clearly establish the effect of confinement on the nonlinearities below bandgap, we have undertaken a systematic study by using a set of SDG samples which present a wide range of nanocrystal sizes (from 2 to 14 nm) and which cover the whole interval of accessible ratios $y = E_g/(\hbar\omega)$, where E_g is the energy gap of the SDG and $\hbar\omega$ is the energy of the incident photon, between 1 and 1.9. The first step in our study is a careful structural characterization of the SDG samples by using the small-angle-neutron scattering (SANS) technique.[13] The SANS data give the crystal size R and the volume fraction f_v occupied by the nanocrystals. The knowledge of f_v is very important because it permits to derive from the optical measurements the nonlinear susceptibility of the crystallite, which is the relevant quantity from the physical point of view.

In order to measure the real and imaginary parts of $\chi^{(3)}$ we used a combination of different nonlinear optical techniques: nonlinear transmission,[14] degenerate-four-wave-mixing (DFWM)[15] and three-wave-mixing.[16] We found that it is very important, in the interpretation of the experimental data, to take into account the effects due to the presence of free carriers generated by two-photon-absorption. In some cases the refraction due to free carriers (which is a fifth-order and not third-order process) represents the dominant effect in DFWM. However, since the relaxation time of the e-h population is in the nanosecond time scale, this process is not very useful for fast devices.

The values of $\chi^{(3)}$, and also of the refractive index change per carrier, that we obtain for the nanocrystals are comparable to those of the bulk semiconductors of similar composition. This indicates that the confinement effects on the nonlinearities, at least in the investigated size range, are small.

2. Materials and Methods

The list of used SDGs, all manufactured by Schott Glaswerke (Mainz, Germany) and commercialized as sharp cut-off optical filters, is given in Table 1. The number

Table 1. S
in the varic
energy-gap
is derived b
of the third-
index chang
β of fourth
dielectric fu

Sample	R [nm]
GG495	2.
OG570	3.
OG590	3
RG610	3.
RG630	3.
RG665	6.
RG695	4.
RG715	5.
RG830	5.
RG850	1
V1	5
V2	7
V3	8
V4	13
R1	4
R2	6
R3	9.
R4	1
PGM	-
NTM	-

which ide
with an u
difference
whereas t
With the
mercial gl
consisting
second, lal
ples have t
because th
also studie
ductor co
non-treate
thermally

Table 1. Second and third column: radius R and volume fraction f_v of the crystallites contained in the various SDG explored (the last two glasses do not contain crystallites). Fourth column: energy-gap E_g. Fifth column: TPA coefficient; when a range of β values is given, the first value is derived by taking $\Sigma = 2 \times 10^{-18}$ cm^2, and the second by taking $\Sigma = 0$. Sixth column: modulus of the third-order susceptibility $|\chi^{(3)}_{\mathrm{SDG}}|$ of the SDG. The last three columns refer to the refractive-index change/e-h density: of SDG (seventh column) derived by making use of the first value of β of fourth column; of nanocrystals (eighth column); predicted for bulk by the plasma-modified dielectric function model (ninth column).

Sample	R [nm]	$f_v\ \lambda$ 10^3	E_g [eV]	$\beta_{\mathrm{SDG}} \times 10^3$ [cm/GW]	$\lvert\chi^{(3)}_{\mathrm{SDG}}\rvert \times 10^{22}$ [m^2/V^2]	$\lvert\sigma_{\mathrm{SDG}}\rvert \times 10^{21}$ [cm^3]	$\lvert\sigma_c\rvert \times 10^{21}$ [cm^3]	$\lvert\sigma_b\rvert \times 10^{21}$ [cm^3]
GG495	2.1	5.2	2.51		7.44			
OG570	3.5	3.5	2.18	2–8	8.13	1.3	1.9	1.9
OG590	3	4.7	2.10	3–10	8.09	1.6	2.2	2
RG610	3.1	2.9	2.03	4–12	7.91	1.2	1.4	2.1
RG630	3.7	3.2	1.97	9–27	8.24	1.9	2.7	2.3
RG665	6.5	3.5	1.87	15–40	7.95	2	2.9	2.5
RG695	4.3	1.6	1.79	9–25	6.76	2.1	3.1	2.7
RG715	5.5	3.2	1.74	18 ± 3	7.55	2.5	3.7	2.8
RG830	5.3	1.6	1.49	17 ± 3	6.10	1.7	3.1	4.8
RG850	11	1.5	1.46	23 ± 3	6.19	2.2	4	4.8
V1	5.2	4	2.42		7.86			
V2	7.6	3.7	2.41		7.83			
V3	8.7	3.6	2.40		8.16			
V4	13.5	3.4	2.38		8.10			
R1	4.8	1.8	1.50		6.38			
R2	6.9	1.7	1.48		6.17			
R3	9.8	1.7	1.46		5.85			
R4	14	1.6	1.45		5.74			
PGM	–	–	4.3		5.37			
NTM	–	–	3.2		6.69			

which identifies the glass corresponds to the cut-off wavelength λ_c in nanometers, with an uncertainty of ± 6 nm. RG830 and RG850 contain CdTe crystallites (the difference in radius accounts for the small difference of their absorption edges), whereas the glasses of the series OG495 – RG715 contain $CdS_{1-x}Se_x$ crystallites. With the frequency mixing measurements we have investigated, besides the commercial glasses, also two series of four experimental glasses, the first, labelled V, consisting of glasses having the same chemical composition as the OG515, and the second, labelled R, with the composition of the RG850. Within each series the samples have the same composition but they differ in the average size of the nanocrystals because they were annealed at different temperatures using a gradient furnace. We also studied a glass made by the pure glass matrix (PGM), in which no semiconductor constituents were introduced during fabrication, and a glass, here denoted non-treated melt (NTM), of the same composition as RG610, but which was not thermally treated for the crystallite growth.

We have reported in Table 1 the value of the energy gap E_g which is derived for each glass from the measured cut-off wavelength λ_c according to the relation: $E_g = hc/\lambda_c$. The value of E_g is determined by the stoichiometry of the nanocrystals and, to a much lesser extent, by their radius. With respect to a bulk semiconductor of equal composition, the confinement increases E_g by 20–200 meV, depending on the ratio between the size of the crystallites and the exciton radius. We recall that the excitonic Bohr radii are 3, 5.6, and 7.4 nm for CdS, CdSe, and CdTe, respectively.[17–19] The ten commercial glasses cover a range of E_g between 1.46 and 2.5 eV. They are all transparent at 1.06 μm ($\hbar\omega = 1.17$ eV), and most of them present appreciable TPA at this wavelength.

The average radius of the nanocrystals and the volume fraction f_v occupied by the nanocrystals were measured by small-angle-neutron-scattering (SANS). Neutron scattering represents a very useful technique for the structural characterization of SDGs because of the strong mismatch in the neutron scattering amplitude between the nanocrystals and the glass matrix.[13,20] The SANS data were taken at the Cold Neutron Facility of the National Institute of Standards and Technology, Gaithersburg, Maryland, USA. Details on the SANS experiment are reported in Ref. 13. The average crystallite radius R is derived from the angular dependence of the scattered intensity, and the volume fraction occupied by the crystallites is obtained from the absolute value of the scattered intensity which is proportional to $f_v R^3$. It should be noted that f_v cannot be derived from a chemical analysis of the SDGs because a significant fraction of the semiconductor constituents is still dispersed in the glass matrix. The measured values of R and f_v are reported in Table 1. We see that R varies in the range 2–14 nm and f_v is in the range $1.5\text{–}5.2 \times 10^{-3}$. As discussed in Ref. 13, the SANS data do not contain direct information about the width of the size distribution, but there is some evidence that the size distribution follows the law predicted by Lifshitz and Slyozov.

The nonlinear optical measurements were performed by using an actively-passively mode-locked Nd:YAG oscillator, operated at 1 Hz, which provides a train of 7–8 pulses at $\lambda = 1.064$ μm. A single pulse with an energy of approximately 0.1 mJ is selected in the early part of the train and amplified to about 10 mJ with negligible distortion. The procedure gives an almost transform-limited pulse. Indeed, we measured through second-harmonic correlation a pulse duration $\tau_p = 28$ ps, and a spectral width $\Delta\lambda = 0.07$ nm (both values represent full width at half maximum) for a time-bandwidth product of 0.5 (to be compared with the value 0.44 predicted for a transform-limited Gaussian pulse). The beam quality factor, obtained by monitoring the transversal intensity profile of the laser beam with a CCD camera, was $M^2 = 1.25$.

In the case of the nonlinear transmission measurements we also performed some experimental runs at the European Laboratory for Nonlinear Spectroscopy, Florence, Italy, where we used a dye laser operating at 605 nm ($\hbar\omega = 2.06$ eV) which provided a 190-fs pulse, with a spectral width of 4.2 nm and repetition rate of 10 Hz.

3. Bulk Nonlinearities and Dielectric Confinement Effects

The nonlinear optical measurements described in this paper permit to derive the third-order susceptibility of the composite, $\chi^{(3)}_{\mathrm{SDG}}(\omega,\omega,-\omega)$. If f_v is small, the approximate relation connecting $\chi^{(3)}_{\mathrm{SDG}}$ to the third-order susceptibility) of the nanocrystals, $\chi^{(3)}_c$, is[1]:

$$\chi^{(3)}_{\mathrm{SDG}} = \chi^{(3)}_g + f_v f^4 \chi^{(3)}_c \,, \tag{1}$$

where $\chi^{(3)}_g$ is the third-order susceptibility of the glass matrix, and f is the local field correction factor. In the visible region $\chi^{(3)}_g$ is a real quantity, whereas $\chi^{(3)}_c$ presents also an imaginary part when the photon energy $\hbar\omega$ is larger than $E_g/2$, that is, when two-photon absorption processes can occur. Assuming a spherical shape and an isotropic polarizability for the crystallites, f is given by: $f = 3n_g^2/(n_c^2 + 2n_g^2)$, where n_g is the index of refraction of the glass matrix and n_c that of the crystallite. At $\lambda = 1.06$ μm, f is calculated by taking: $n_g = 1.53$ (from Ref. 21); $n_c = 2.84$ (value of bulk CdTe) for RG830 and RG850; $n_c = 2.33$ (value of bulk CdS) for GG495, $n_c = 2.54$ (value of bulk CdSe) for RG715 (bulk data from Ref. 22) and then interpolating according to λ_c for the other glasses of the CdSSe series. At 0.6 μm, n_c is about 3% larger and f^4 somewhat lower.

It should be noted that the effect of non-sphericity of the nanocrystals on f^4 is likely to be small. In fact, a strong shape asymmetry is required to significantly change the polarizability tensor components of a single particle, and these changes are smoothed out in averaging over the random orientations of the crystallites.

The main of our investigation was to derive $\chi^{(3)}_c$, and to compare it with the bulk value $\chi^{(3)}_b$ in order to understand whether confinement plays a role in the frequency region below the bandgap of the semiconductor.

A large body of work, both experimental and theoretical, has been done on $\chi^{(3)}_b$ of bulk semiconductors, in particular for TPA. For TPA, as discussed in Ref. 5, experimental data are in agreement with the relation:

$$\mathrm{Im}\,\chi^{(3)}_b = c_1(1/\omega E_g^3)(2\hbar\omega/E_g - 1)^{3/2}(2\hbar\omega/E_g)^{-5} \,, \tag{2}$$

where E_g and $\hbar\omega$ are the band-gap and the photon energy, respectively, while the constant c_1 is practically independent from the specific material. Concerning the real part, Sheik-Bahae *et al.*,[5,6] by adopting a Kramers-Kronig approach, proposed an expression that accounts fairly well for the behavior of the nonlinear refraction with the band-gap of various semiconductors. Converted to our notation, the expression can be written as:

$$\mathrm{Re}\,\chi^{(3)}_b = c_2 E_g^{-4} G_2(\hbar\omega/E_g) \,. \tag{3}$$

The algebraic expression for $G_2(y)$ and the value of the constant c_2 are given in Ref. 6. $\mathrm{Re}\,\chi^{(3)}_b$ peaks for $\hbar\omega/E_g \approx 0.55$, vanishes at $\hbar\omega/E_g \approx 0.7$ and becomes negative for larger values of $\hbar\omega/E_g$. We notice that, due to their continuously

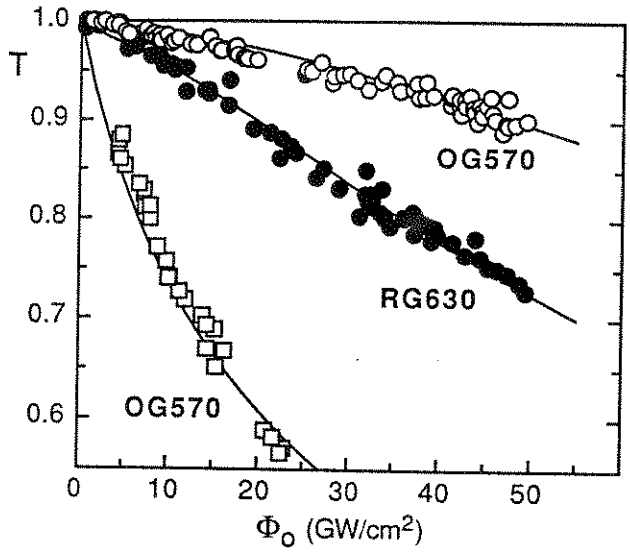

Fig. 1. Transmission versus peak intensity for some SDGs. The two upper sets of data points, (○) and (•) are taken with 28 ps pulses at 1.06 μm with a sample thickness of 0.8 cm. The lower set of data points, (□), is taken with 190 fs pulses at 0.6 μm with a sample thickness of 5 cm. Full lines are best fit curves.

varying stoichiometry, for most CdSSe crystallites there are no direct experimental $\chi_b^{(3)}$ data on the corresponding bulk. Equations (2) and (3) are then quite useful to interpolate among the experimental data.

4. Two-Photon Absorption

We present in Fig. 1 some plots of the transmission T, derived as the ratio between the transmitted energy and the input energy, as a function of the peak intensity Φ_0. The decrease of T with Φ_0 is due to TPA processes. We find indeed that the nonlinearity of the absorption of the Nd:YAG laser pulses becomes undetectable for SDGs with $\lambda_c \leq 550$ nm. It should be noted that the glass matrix, with its large bandgap, plays no role in TPA. In presence of TPA, the intensity Φ of a pulse propagating along z is given, neglecting diffraction, by:

$$\frac{d\Phi(r,z,t)}{dz} = -\beta\Phi^2(r,z,t) - \Sigma N(r,z,t)\Phi(r,z,t)\,, \tag{4}$$

where r is the radial coordinate, and β is the TPA coefficient which is related to $\mathrm{Im}\,\chi^{(3)}$ by the expression: $\beta = \omega(\varepsilon_0 c^2 n^2)^{-1}\mathrm{Im}\,\chi^{(3)}$, n is the index of refraction. The second term at left hand side of Eq. (4) accounts for photon absorption processes due to the presence of free carriers, with N the free carrier density generated by TPA and Σ denoting the related cross-section. Assuming the decay of N to be negligible during the pulse duration (the validity of this assumption is supported by the time-resolved degenerate-four-wave-mixing measurements described in the

following section), N can be calculated through:

$$N(r,z,t) = \int_{-\infty}^{t} \frac{\beta\Phi^2(r,z,t')}{2\hbar\omega}\,dt'. \tag{5}$$

By assigning the spatial intensity profile and the temporal shape of the pulse, the nonlinear dependence of the output energy as a function of the input energy can be calculated by solving numerically Eqs. (4) and (5). In principle, the two parameters β and Σ could be obtained by a best fit to the data taken with a single sample of thickness L. However, because of the limited range of input energies over which the nonlinear transmission can be investigated and because of the uncertainties associated with the experimental data, it is not possible to extract reliably the two parameters from a single experimental curve. For instance, the data points referring to the OG570 sample in Fig. 1 can be described, with no appreciable difference in the quality of the fit, by adopting any couple of values within the interval: $\beta_{\mathrm{SDG}} = 8\times10^{-3}$ cm/GW, $\Sigma = 0$; $\beta_{\mathrm{SDG}} = 2\times10^{-3}$ cm/GW, $\Sigma = 2\times10^{-8}$ cm^2. It should be noted that, for $\Sigma = 0$, the transmission derived from Eq. (2) depends on the peak intensity Φ_0 and on L only through the product $\Phi_0 L$.[14] Therefore, by plotting T vs $\Phi_0 L$ for different sample thicknesses, one can investigate whether FCA is playing some role and one can derive without ambiguity both β_{SDG} and Σ. Adopting this procedure, we estimated $\Sigma \approx 2\times10^{-8}$ cm^2 for both RG830 and RG715. Such a value is consistent with $\Sigma = 1.95\times10^{-18}$ cm^2, as derived for RG850 in Ref. 9.

A simple way to reduce the effect of FCA is that of measuring the nonlinear transmission with ultrashort pulses which can provide a high enough intensity to make evident TPA without exciting too many carriers during the pulse duration. Numerical solutions of Eqs. (4) and (5) indicate that, for an extended range of values of L, Φ_0, and Σ, the effect of FCA can safely be disregarded with pulses as short as 190 fs. Our ultrashort-pulse investigation was limited to GG495, OG570 and OG590, because only the wavelength of 605 nm was available at the time of the experiment. The 190 fs pulse from the dye laser amplifier, after passing through a spatial filter, was gently focused to provide $\approx$10 μJ of energy within a smooth Airy disc at the sample. A good accuracy in the measurement of T was achieved by using a differential detector and a reference beam. A crosscheck of the absolute calibration (which required measuring energy, beam shape, and pulse duration) was given by a separate experiment in which we observed the beam depletion due to second-harmonic generation in a 0.5-mm-thick KDP platelet, in type-I phase matching (using KDP as a TPA standard, we assumed d_{36} (KDP) = 0.4 pm/V). Since beam depletion due to second-harmonic generation is formally equivalent to that due to TPA, such a calibration procedure is simple and reliable. We found some evidence of a darkening effect[1] (especially with GG495): that is, starting with a fresh sample, the linear transmission showed an initial decrease with time before stabilizing after exposure. We relied on pre-darkening to avoid changes of the linear transmission during data collection. A typical transmission curve can be seen in Fig. 1.

The values of β_{SDG} derived from the measurements performed with 28 ps pulses at 1.06 μm are reported in Table 1. For those cases in which it was not possible to derive both β and Σ, we fixed Σ by considering the two extreme scenarios of $\Sigma = 2 \times 10^{-18}$ cm^2 and $\Sigma = 0$. There is some indication[9] that Σ decreases as E_g increases, so that the value $\Sigma = 0$ is probably the more appropriate for the largest values of the ratio $E_g/(\hbar\omega)$.

The few published values of β_{SDG} are rather different among themselves and are all larger than our data. The origin of the discrepancy with some of the previous works is probably that FCA was not taken into account in the interpretation of transmission data, a fact that becomes more disturbing with the longer laser pulses. The discrepancy with Ref. 9, where the effect of FCA was considered, is within a factor 2, which is not that large for a TPA measurement.

By using Eq. (1), we can write: $\beta_{SDG} = \beta_c\ (n_m^2/n_{SDG}^2) f^4 f_v$. This relation allows to derive β_c from the measured β_{SDG} and f_v. Taking into account all the uncertainties, we estimate that the absolute calibration of β_c in our experiment is correct within a factor 2. From β_c we obtain $\mathrm{Im}\,\chi_c^{(3)}$.

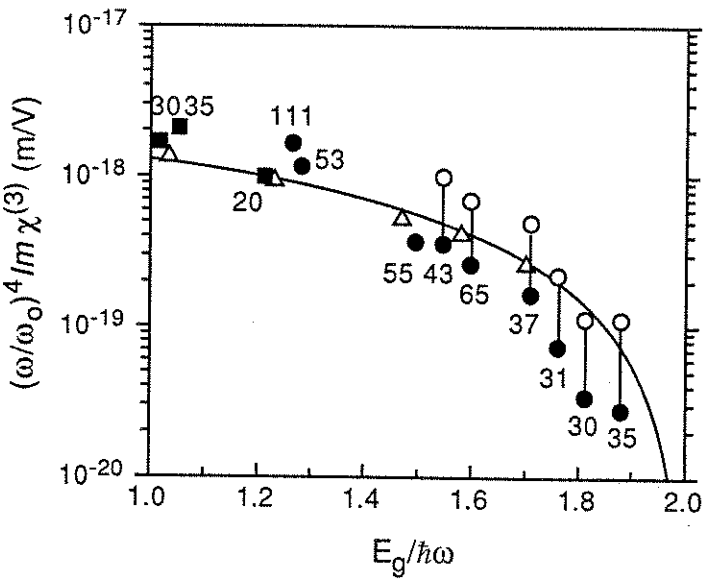

Fig. 2. Plot of the scaled quantity $(\omega/\omega_0)^4 \mathrm{Im}\,\chi^{(3)}$ versus $E_g/(\hbar\omega)$. (■): optical measurements at 0.6 μm. Circles refer to optical measurements at 1.06 μm assuming: $\Sigma = 2 \times 10^{-18}$ cm^2 (•), $\Sigma = 0$ (○). The numbers associated to the experimental points are the radii of the nanocrystals in Ångströms. (△): experimental data for bulk semiconductors, taken from Refs. 7 and 23, all measured at 1.06 μm, except for the point corresponding to the lowest value of $E_g/(\hbar\omega)$ which is measured at 0.53 μm. The solid line is the behavior of $(\omega/\omega_0)^4 \mathrm{Im}\,\chi^{(3)}$ predicted for bulk semiconductors by Eq. (2).

The comparison between the TPA coefficient of nanocrystals and that of bulk semiconductors is shown in Fig. 2, where we plotted the scaled quantity $(\omega/\omega_0)^4 \mathrm{Im}\,\chi_c^{(3)}$, with ω_0 the frequency of 1.06 μm radiation, as a function of $y = E_g/(\hbar\omega)$. The full curve in Fig. 2 gives the bulk values, calculated by using Eq. (2). The constant in the expression of $\mathrm{Im}\,\chi_b^{(3)}$ is fixed by fitting the curve to experimental data for bulk semiconductors[7,23] which are also reported in Fig. 2.

5. Degenerate Four-Wave Mixing

The experimental set-up was arranged according to the standard backward DFWM configuration.[24] We used the same pulsed mode-locked Nd:YAG laser utilized for the TPA experiment. After passing through a variable attenuator, the beam was gently focussed by a long focal length optics, and then being splitted into pumps and probe. Images recorded with a CCD camera and transmission through pin-holes of various diameters indicated that the spatial profile at the focussing waist, where the samples were located, could be fairly well fitted with a Gaussian distribution of radius $w_0 = 0.86$ mm at $1/e^2$ intensity (an additional 10% energy was present beyond 1.1 w_0, but these far out wings did not play any role in our experiment). We denote with f and b the forward and backward pump; with p the probe and with c the phase-conjugated reflected pulse; with W_i the energy of the pulse specified by the label; with b and p the ratios: $b = W_b/W_f$, $p = W_p/W_f$. All the measurements here reported have been taken with fixed b and p ($b \approx 1$ and $p \approx 1/10$). The reflectivity R is defined by $R = W_c/W_p$. The angle θ between f and p was small enough ($\theta = 5°$) to guarantee a good overlapping of pumps and probe throughout the 3 mm thickness of the samples. We made an absolute calibration of the set up. A confirmation to this calibration came from measurements of the DFWM reflectivity for a sample of BK7 glass: we obtained $|\chi^{(3)}| = 3.8 \pm 0.7 \times 10^{-22}$ (MKS unit) in fair agreement with the values (3.9–4.6×10^{-22}) reported in the literature.

We denote by Φ_0 the peak intensity of the forward pump. Even at the maximum intensity used ($\Phi_0 \approx 1.6$ GW/cm^2) the depletion of the pulses by TPA (and by the subsequent free carrier absorption) was negligible.

A set of measurements of the reflectivity R versus Φ_0 is reported in Fig. 3. The data are taken with the pulses in coincidence and with parallel polarizations. A pure third order response, with $R \propto \Phi_0^2$, is observed in OG550 and in other glasses with larger gap, whereas the reflectivity scales according to $R \propto \Phi_0^4$ for RG630 ($E_g \approx 2$ eV) and for all the other SDGs presenting E_g smaller than that of RG630. The behavior $R \propto \Phi_0^4$ can be explained by refraction due to real excitations generated by TPA. Indeed the reflectivity is larger for the glasses presenting a larger two-photon absorption coefficient β. The lower β is, the higher is the minimum intensity necessary to observe the fifth order nonlinearity. The data of Fig. 3 indicate that for OG590 the fifth order nonlinearity becomes dominant above 0.5 GW/cm^2 and for OG570 it gives some contribution only above 1 GW/cm^2. Some TPA occur also in OG550, but, since β is very small for this glass, the e–h refraction

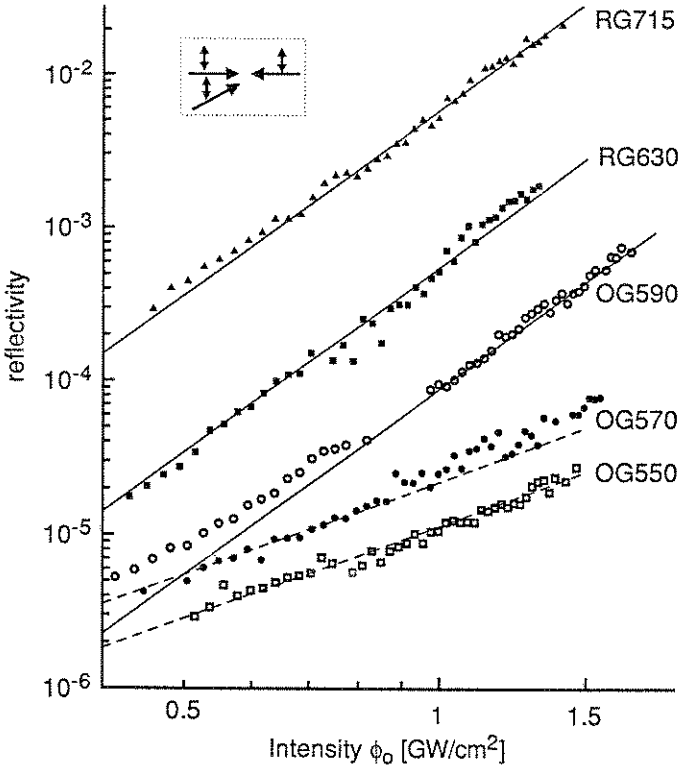

Fig. 3. Reflectivity versus intensity for some SDGs. Data are taken with f, b, p in temporal coincidence and with parallel polarizations. Sample thickness: 3 mm. Full lines: $R \propto \Phi_0^4$; dotted lines $R \propto \Phi_0^2$.

was not evident at the intensities used in our experiment, and only the third-order reflectivity was observed. We found no evidence of saturation of the fifth order nonlinearity in any of the glasses where the effect was present.

Starting from a fresh sample, we did not observe changes of the reflectivity, or of decay times, after a prolonged exposure at the maximum intensity.

Time resolved measurements were accomplished with f and p in coincidence and b delayed by a time interval Δ. Measurements of R versus Δ with different polarizations are discussed in great detail in Ref. 15. We show in Fig. 4 some data obtained with the two glasses RG715 and RG850. The data have been taken with a thin sample, $L = 0.5$ mm, in order to avoid even a minimal beam depletion and any possible effect due to the finite transit time of the pulses in the sample. Actually, runs performed on a 3-mm thick sample of the same glass gave similar plots, with R scaling as L^2. Figure 4 shows that the decay of the reflectivity after excitation occurs on the nanosecond time scale which is the time scale for the decay of the electron-hole population.

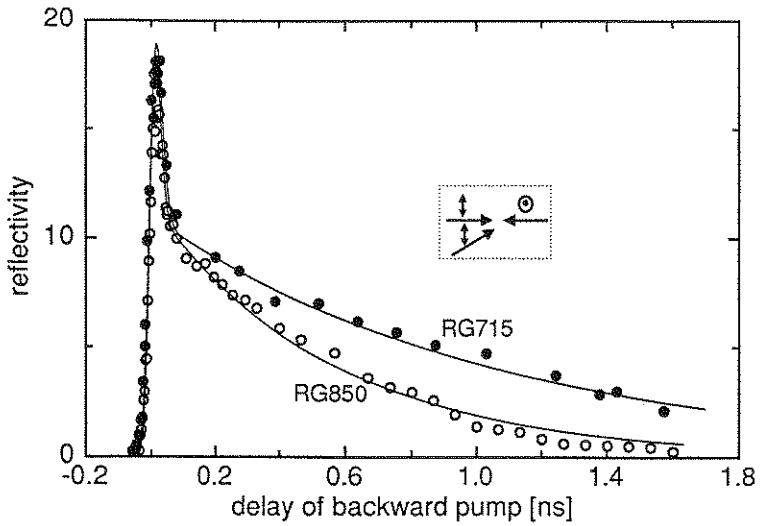

Fig. 4. Reflectivity versus delay Δ. Intensity: $\Phi_0 \approx 1.5$ GW/cm^2. Samples: 0.5-mm-thick RG850 and RG715. Polarizations: b perpendicular to f and p. The vertical scale is not the same for the two glasses.

It is important to remark that the peak in the reflectivity which is observed around zero delay is not due to a fast third order effect, but rather to the enhanced TPA which occurs when f and b are simultaneously present. In fact, the full curves appearing in Fig. 4 represent a best-fit of calculations[15] performed under the hypothesis that the effect is only determined by free-carriers refraction. Our calculations have assumed that, similarly to the case of bulk semiconductors, the change of refractive index is proportional to the e-h density N : $\Delta n = \sigma N$. The imaginary part of σ arises from the linear absorption of the carriers. Taking $\Sigma = 2 \times 10^{-18}$ cm^{-2}, we estimate $\mathrm{Im}\,\Delta n/|\Delta n| = \mathrm{Im}\,\sigma/|\sigma| \approx 10^{-2}$. For DFWM below band-gap, one can then assume σ to be real. The best fit to the DFWM data gives the product $\beta_{\mathrm{SDG}}|\sigma_{\mathrm{SDG}}|$ for each glass. Since β_{SDG} is known from the TPA measurements, we can obtain $|\sigma_{\mathrm{SDG}}|$. The sign of σ_{SDG} cannot be obtained through DFWM, which only measures the modulus. Clear indications that σ_{SDG} is negative were obtained from Z-scan measurements performed on RG715 and RG850, always employing the same laser pulse at 1.06 μm.

inside the crystallites. It is important to derive the response σ_c of the crystallites themselves, since this quantity is directly related to the physical processes involved.

The relation between σ_{SDG} and σ_c can be obtained starting from the definition: $\Delta n_c = \sigma_c N_c$, and recalling that $N_{SDG} = f_v N_c$. Correcting for the local field, we obtain:

$$\sigma = \sigma_c \frac{n_c}{n_{SDG}} f^2 . \tag{6}$$

Values of $|\sigma_{SDG}|$ and $|\sigma_c|$ are reported in Table 1, together with σ_b, the refractive index change per e-h pair in the bulk semiconductors. Since experimental data are available in the literature only for CdTe, we have reported for the bulk CdSSe semiconductors the values of σ_b predicted by the plasma-modified dielectric function model (differences with the predictions of other models are irrelevant when compared with present accuracy),[4,7] according to which: $\sigma_b = -e^2/(2m_{eh}\varepsilon_0 n\omega^2)E_g^2/[E_g^2 - (\hbar\omega)^2]$, with m_{eh} the reduced effective e-h mass, E_g the band-gap and ω the optical frequency. From the known values of m_{eh} and E_g,[22] we calculated $\sigma_b \cong -3 \times 10^{-21}$ cm^3 for CdSe and $\sigma_b \cong -1.5 \times 10^{-21}$ cm^3 for CdS. For the mixed semiconductors, σ_b was derived by linear interpolation according to the cut-off wavelength.

One notices that the values of $|\sigma_c|$ and $|\sigma_b|$ are comparable. In view of the discussed uncertainties in β, the comparison is more significant for RG850, RG830 and RG715 (in particular, for the two CdTe glasses, we can rely on an experimental value for σ_b). For the CdSSe series the magnitude and the decrease of $|\sigma_c|$ moving from RG715 ($E_g = 1.7$ eV) to RG570 ($E_g = 2.2$ eV) are in broad agreement with the prediction for the bulk.

For technical reasons we could not operate at intensities sufficiently low to measure $|\chi^{(3)}|$ in all glasses. We could observe a pure third order nonlinearity only in the case of OG495, OG515 and OG550. For these glasses the DFWM reflectivity was only 2–3 times that of a borosilicate glass, consistent with the more accurate measurements reported in the next section.

6. Three-Wave Mixing

We have seen in the previous section that the DFWM technique measures a nonlinear susceptibility which includes the contribution of the free carriers generated by TPA. Such a contribution, which corresponds to a fifth-order nonlinearity,obscures the true third-order effect and makes it difficult to derive accurate values of Re $\chi^{(3)}_{SDG}$ whenever $E_g < 2\hbar\omega$. To avoid the problem of free-carriers refraction, we have performed a non-degenerate wave mixing experiment. The scheme of the experiment is shown in the inset of Fig. 5: pulse a (of frequency ω_a) is mixed in the sample with pulse b (frequency $\omega_b = \omega_a - \Delta$) to yield pulse c at the new frequency $\omega_c = 2\omega_a - \omega_b$. By using Δ^{-1} much smaller than the carriers recombination time, the free carriers give no appreciable contribution to the index of refraction grating. The 28-ps pulse was generated by the same Nd:YAG mode-locked laser used in the experiments described in the previous sections. Part of the pulse directly provided a, while part

of it was red-shifted (≈ 250 cm^{-1}) by Stimulated Raman Scattering to provide b. Pulses a and b were collinear and co-polarized. An adjustable delay allowed for their temporal synchronization. At the sample, beam a could be well approximated by a Gaussian profile with a 2.2 mm spot-size at FWHM intensity, while b was collimated to a smaller spot of 0.44 mm, so that it could be easily centred within that of a. Beam b was not diffraction limited, its divergence was ≈ 5 mrad. Typical values of the peak intensity was $\Phi_a \approx 1$ GW/cm^2 and $\Phi_b \approx 40$ MW/cm^2. Pulse c was detected by a photomultiplier; a monochromator plus narrow-band interferential filters were used to reject a and b. At each shot, the energies of the impinging pulses, W_a and W_b, were recorded with the energy of the generated pulse W_c. Platelets of BK7 glass of various thicknesses were used as a reference.

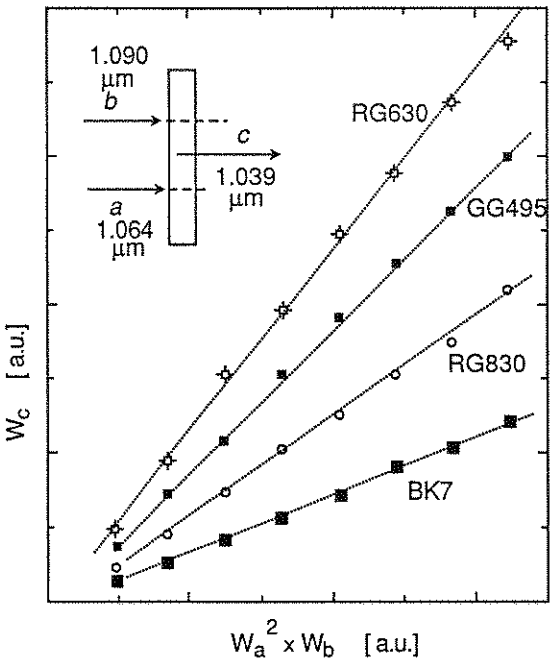

Fig. 5. Plot of W_c versus $W_a^2 W_b$ for some glasses. The inset shows the experimental scheme.

Assuming infinite plane waves propagating along z, slowly varying envelope approximation, assuming negligible the depletion of a and the gain of b, denoting by n_i is the index of refraction at frequency ω_i, the intensity of c at the exit of a sample of thickness L is:

$$\Phi_c = \frac{n_a^2}{n_b n_c} \sin c^2 \left(\frac{\Delta h L}{2} \right) \left[\frac{|\chi^{(3)}| L \omega_a}{2\varepsilon_0 c^2 n_a^2} \right]^2 \Phi_\alpha^2 \Phi_b \,. \tag{7}$$

If we limit our treatment to the case $\Delta h L \ll 2\pi$. Eq. (7) can be written in terms of pulse energies as:

$$W_c = A |\chi^{(3)}|^2 n_a^{-4} L^2 W_\alpha^2 W_b \tag{8}$$

where the shape and the overlapping of the pulses, in time and space, are taken into account by the constant A.

We found that, up to $L = 4$ mm, W_c followed reasonably well the L^2 dependence, a fact which granted the validity of the approximation $\Delta hL \ll 2\pi$ (the mismatch Δh was mostly due to the divergence of b rather than to frequency dispersion). We show in Fig. 5 some examples of the observed behavior of W_c versus $W_a^2 W_b$. The used intensities were low enough, so that no attenuation of a (and b) due to TPA could be detected in any investigated glass. Indeed, the linearity of the plots in Fig. 5 is quite indicative to this regard. Noting from Eq. (8) that the slope of the straight lines of Fig. 5 is proportional to $|\chi^{(3)}|^2$, and comparing with the slope measured with reference BK7 platelets of the same thickness, we derived for each glass the ratio between $|\chi^{(3)}_{\mathrm{SDG}}|$ and $|\chi^{(3)}_{\mathrm{BK7}}|$. The absolute values of $|\chi^{(3)}_{\mathrm{SDG}}|$ reported in Table 1 are calculated by assuming $|\chi^{(3)}_{\mathrm{BK7}}| = 4.5 \times 10^{-22}$ m^2/V^2. One can notice that the modulus of the third order susceptibility of the SDGs is comparable to that of the glass matrix.

$|\mathrm{Re}\,\chi^{(3)}_{\mathrm{SDG}}|$ is readily derived from the relation: $|\mathrm{Re}\,\chi^{(3)}_{\mathrm{SDG}}|^2 = |\chi^{(3)}_{\mathrm{SDG}}|^2 - |\mathrm{Im}\,\chi^{(3)}_{\mathrm{SDG}}|^2$. Values of $\mathrm{Im}\,\chi^{(3)}_{\mathrm{SDG}}$ can be obtained from the TPA measurements described above. Since we have used in this latter experiment also glasses which were not studied in the nonlinear transmission experiment, in the actual calculation of $|\mathrm{Re}\,\chi^{(3)}_{\mathrm{SDG}}|$, we have used, instead of the direct TPA results, values of $\mathrm{Im}\,\chi^{(3)}_{\mathrm{SDG}}$ derived from the full curve in Fig. 2 which interpolates very well the experimental data. $|\mathrm{Re}\,\chi^{(3)}_{\mathrm{SDG}}|$ turns out to be quite close to $|\chi^{(3)}_{\mathrm{SDG}}|$, that is, $|\mathrm{Re}\,\chi^{(3)}_{\mathrm{SDG}}|^2 \gg |\mathrm{Im}\,\chi^{(3)}_{\mathrm{SDG}}|^2$ for all glasses. Considering, for instance, the glasses with CdTe nanocrystals (which present the largest two photon absorption), we find that $|\mathrm{Im}\,\chi^{(3)}_{\mathrm{SDG}}|^2$ is ten times smaller than $|\chi^{(2)}_{\mathrm{SDG}}|$. We note that the values we find for $|\mathrm{Re}\,\chi^{(3)}_{\mathrm{SDG}}|$ are much smaller than those reported in Refs. 8 and 12. In order to obtain information on the sign of $\mathrm{Re}\,\chi^{(3)}_{\mathrm{SDG}}$, we have repeated the experiment by employing "stacking samples" (an SDG of thickness L_{SDG} in contact with a BK7 platelet of thickness L_{BK7}). This allows to measure the quantity $|L_{\mathrm{SDG}}\chi^{(3)}_{\mathrm{SDG}} + L_{\mathrm{BK7}}\chi^{(3)}_{\mathrm{BK7}}|^2$. For all glasses the signal increased by adding the BK7 platelet. Since $\chi^{(3)}_{\mathrm{BK7}}$ is real and positive, this implies that $\mathrm{Re}\,\chi^{(3)}_{\mathrm{SDG}} > 0$. We then have both sign and magnitude of $\mathrm{Re}\,\chi^{(3)}_{\mathrm{SDG}}$. From the point of view of the comparison with theory, the quantity of physical interest is $\chi^{(3)}_c$, the nonlinear susceptibility of the nanocrystals. By using Eq. (1), we obtain

$$\mathrm{Re}\,\chi^{(3)}_c = \frac{\mathrm{Re}\,\chi^{(3)}_{\mathrm{SDG}} - \chi^{(3)}_g}{f_v f^4} \,. \tag{9}$$

In order to derive $\mathrm{Re}\,\chi^{(3)}_c$ from the measured $\mathrm{Re}\,\chi^{(3)}_{\mathrm{SDG}}$ by using Eq. (9), we need the exact value of $\chi^{(3)}_g$, the susceptibility of the matrix after the thermal treatment. It is reasonable to approximate $\chi^{(3)}_g$, which cannot be measured, by $\chi^{(3)}_{\mathrm{PGM}}$ or $\chi^{(3)}_{\mathrm{NTM}}$. Between the two values (which are quite close, as shown in Table 1), it seems more appropriate to choose $\chi^{(3)}_{\mathrm{NTM}}$ (at least for the CdSSe glasses),

since most of the semiconductor components of the melt are not incorporated in the crystallites during the thermal treatment for crystal growth. We set for all glasses $\chi_g^{(3)} = \chi_{\mathrm{NTM}}^{(3)} = 6.7\ \mathrm{m^2/V^2}$. We plotted $\mathrm{Re}\,\chi_c^{(3)}$ versus $\hbar\omega/E_g$ in Fig. 6. The solid line in the same figure represents $\mathrm{Re}\,\chi_b^{(3)}$ for the bulk calculated from Eq. (3). To fit the calculated curve with the experimental data, we had to use a value of c_2 smaller by a factor 0.6 than suggested in Ref. 6. Because of the uncertainties in the

erable effort is still devoted to the assessment of the energy levels in semiconductor crystallites. Early calculations of energies and wavefunctions of the discrete levels were based on the two-band effective-mass approximation. For the quantitative interpretation of the absorption/fluorescence spectra, models were improved by taking into account valence-band mixing.[25] A tight binding approach to go behind the effective mass approximation has been pursued by Ramaniah *et al.*[26] Such a theoretical description of the energy levels might eventually lead to accurate predictions of dispersion and magnitude of $\chi_c^{(3)}$, although for the moment only preliminary results are available.

With the aim to obtain the broad features of $\chi_c^{(3)}$ versus R, Cotter *et al.*[8] have used a simplified approach based on the two-band effective-mass approximation, and on a truncated sum-over-states. Their calculations predict for nanocrystals a significant decrease of the TPA cross-section as R is reduced, a more modest because of $\mathrm{Re}\,\chi_c^{(3)}$ and a negative sign for $\mathrm{Re}\,\chi_c^{(3)}$. The origin of the behavior of $\mathrm{Re}\,\chi_c^{(3)}$ is attributed to the fact that the processes associated to the optical Stark effect are much less affected by the reduced size than those related to TPA. Our data do not seem to support this picture.

Figure 2 shows that $\mathrm{Im}\,\chi_c^{(3)}$ decreases monotonically as y increases. Within experimental errors, TPA in the nanocrystals has the same behavior as in the bulk semiconductor. Effects of confinement on $\mathrm{Im}\,\chi_c^{(3)}$ must be small, if we note that deviations from the bulk values are not evident even for the small crystallites of the GG495 glass ($R = 2$ nm). The same conclusion applies to $\mathrm{Re}\,\chi_c^{(3)}$: it is positive for small values of $\hbar\omega/E_g$, and changes its sign for $\hbar\omega/E_g$ larger than 0.75, as expected for the bulk. Within the present experimental accuracy, Eqs. (2) and (3) seem adequate to account for the magnitude and dispersion of $\chi_c^{(3)}$ for crystallites of a few nanometers size.

The main result of DFWM measurements was to clearly demonstrate the effect of free carrier refraction. We find that crystallites behave also in this respect as the bulk. It is interesting to compare σ below band-gap with σ at resonance. Converting to present notation the value of σ_{eff} given in Ref. 27 (obtained at resonance in glasses similar to RG695), we derive $|\sigma_{\mathrm{resonance}}| \approx 5 \times 10^{-21}$ cm^3. This value is 2.5 times larger than the one we find below band-gap. One of the reasons for the modest increase of σ at resonance can probably be attributed to the large phonon-broadening of the discrete levels.

In our opinion, the fact that σ_c takes, in the SDG, a value similar to that found in the bulk semiconductor, is somewhat expected below band-gap. In the bulk semiconductor, the refractive index change is due to blocking and plasma effects (the two contributions are comparable in bulk CdTe).[7] In the crystallite, the energy levels are discrete and the oscillator strengths of the valence-conduction band transitions concentrate in discrete lines. However, when $E_g - \hbar\omega$ is larger than the separation of the discrete energy levels, as it occurs in our case, this redistribution of oscillator strengths is expected to have a minor role in the sum-over-states calculations leading to the linear susceptibility and to the blocking effect. The same argument applies

to the plasma contributions, for which one expects to recover the Drude expression also in nanocrystals whenever $\hbar\omega$ is larger than the energy spacing due to the confinement. This is shown in Ref. 28 for metal particles. From the same reference we infer that the imaginary part of the plasma contribution, which arises from the limited free path of the electron (and of the hole) in the nanocrystal, is irrelevant in our experiment.

As a final remark, we notice that some features of quantum confinement might have been obscured or smoothed out by the polydispersity and the imperfections which are intrinsic to SDGs. It should be mentioned that new techniques for the preparation of high-quality nearly monodisperse samples of nanometer size II–VI semiconductor crystallites have been recently developed.[29] These new techniques should yield samples which are better characterized than SDGs from the point of view of polydispersity in size and shape, surface defects, degree of crystallinity, and chemical composition of the nanocrystals. We believe that it would be worthwhile to repeat the nonlinear optical experiments on those new samples.

Acknowledgements

We thank B. Speit (Schott, Mainz, Germany) for the gift of SDG samples, and the European Laboratory for Nonlinear Spectroscopy, in particular R. Righini and E. Sa'nta, for making available the femtosecond laser equipment. We acknowledge financial support from the Italian Ministry for University and Research (MURST 40% funds) and from the project "Ottica guidata nonlineare" of the Consiglio Nazionale delle Ricerche (Italy).

References

1. For a review, see: C. Flytzanis, F. Hache, M. C. Klein, D. Ricard, and P. Roussignol, *Progr. Optics* **29**, 323 (1991).
2. N. Finlayson, W. C. Banyai, C. T. Seaton, G. L. Stegeman, M. O'Neill, T. G. Cullen, and C. N. Ironside, *J. Opt. Soc. Am.* **B6**, 675 (1989).
3. J. Yumoto, S. Fukushima, and K. Kubodera, *Opt. Lett.* **12**, 832 (1987).
4. R. K. Jain and M. B. Klein, *Optical Phase Conjugation*, ed. R. A. Fisher (Academic Press, New York, 1983).
5. M. Sheik-Bahae, D. J. Hagan, and E. W. Van Stryland, *Phys. Rev. Lett.* **65**, 96 (1990).
6. M. Sheik-Bahae, D. C. Hutchings, D. J. Hagan, and E. W. Van Stryland, *IEEE J. Quantum Electron.* **27**, 1296 (1991).
7. E. J. Canto-Said, D. J. Hagan, J. Young, and E. W. Van Stryland, *IEEE J. Quantum Electron.* **27**, 2274 (1991); A. A. Said, M. Sheik-Bahae, D. J. Hagan, T. H. Wei, J. Young, and E. W. Van Stryland, *J. Opt. Soc. Am.* **B9**, 405 (1992).
8. D. Cotter, M. G. Burt, and R. J. Manning, *Phys. Rev. Lett.* **68**, 1200 (1992).
9. S. M. Oak, K. S. Bindra, R. Chari, and K. C. Rustagi, *J. Opt. Soc. Am.* **B10**, 613 (1993).
10. R. Tommasi, M. Lepore, and I. M. Catalano, *Solid State Commun.* **85**, 539 (1993).
11. K. I. Kang, B. P. McGinnis, Sandalphon, Y. Z. Hu, S. W. Koch, N. Peyhambarian, A. Mysyrowicz, L. C. Liu, and S.H. Risbud, *Phys. Rev.* **B45**, 3465 (1992).

12. H. L. Fragnito, J. M. Rios, A. S. Suarte, E. Palange, J. A. Medeiros Neto, C. L. Cesar, L. C. Barbosa, O. L. Alves, and C. H. Brito Cruz, *J. Phys.: Condens. Matter* **3**, A179 (1993).
13. G. P. Banfi, V. Degiorgio, and B. Speit, *J. Appl. Phys.* **74**, 6925 (1993); V. Degiorgio and G. P. Banfi, *Nonlinear Optical Materials, Principles and Applications*, eds. V. Degiorgio and C. Flytzanis (IOS Press, Amsterdam, 1995) p. 267.
14. G. P. Banfi, V. Degiorgio, M. Ghigliazza, H. M. Tan, and S. Tomaselli, *Phys. Rev.* **B50**, 5699 (1994).
15. G. P. Banfi, V. Degiorgio, and H. M. Tan, *J. Opt. Soc. Am.* **B12**, 621 (1995).
16. G. P. Banfi, V. Degiorgio, D. Fortusini, and H. M. Tan, *Appl. Phys. Lett.* (1995).
17. L. E. Brus, *J. Chem. Phys.* **80**, 4403 (1984).
18. F. Hache, M. C. Klein, D. Ricard, and C. Flytzanis, *J. Opt. Soc. Am.* **B8**, 1802 (1991); A. I. Ekimov, F. Hache, M. C. Schanne-Klein, D. Richard, C. Flytzanis, I. A. Kudryavtzev, T. V. Yazeva, and A. V. Rodina, *J. Opt. Soc. Am.* **B10**, 100 (1993).
19. J. A. Medeiros Neto, C. Barbosa, C. L. Cesar, O. L. Alves, and F. Galembeck, *Appl. Phys. Lett.* **59**, 2715 (1991).
20. V. Degiorgio, G. P. Banfi, G. C. Righini and A. R. Rennie, *Appl. Phys. Lett.* **57**, 2879 (1990).
21. Data book "*Farb und Filter Glas*" (Schott Glaswerke, Mainz, Germany, 1991).
22. *Information sheet on II-IV compounds* (Cleveland Crystals, Cleveland, Ohio, USA, 1984).
23. E. W. Van Stryland, M. A. Woodhall, H. Vanherzele, and M. J. Soileau, *Opt. Lett.* **10**, 490 (1985).
24. D. M. Pepper and A. Yariv, *Optical Phase Conjugation*, ed. R. A. Fisher (Academic Press, New York, 1983).
25. D. Ricard, *Nonlinear Optical Materials, Principles and Applications*, eds. V. Degiorgio and C. Flytzanis (IOS Press, Amsterdam, 1995) p. 289.
26. L. M. Ramaniah and S. V. Nair, *Phys. Rev.* **B47**, 7132 (1993), and references therein.
27. H. Shinojima, J. Yumoto, and N. Uesugi, *Appl. Phys. Lett.* **60**, 298 (1992).
28. F. Hache, D. Ricard, and C. Flytzanis, *J. Opt. Soc. Am.* **B3**, 1647 (1986).
29. See C. B. Murray, D. J. Norris, and M. G. Bawendi, *J. Am. Chem. Soc.* **115**, 8706 (1993), and references therein.

Journal of Non
Vol. 5, No. 2 (1
© World Scien

MIR

We have c
transverse
the distril
signal anc
beam, one
the oscilla
OPO's an
achieved l
based on
structures
The nond
configurat
pumped c

1. Introduc

Conventiona
lishing oscill
a second-ord
(BOPO's) in
a second-ord
of the OPO'
not required
garded as a r
the mirrorles
stated in Re
has not been